

RESEARCH

Open Access



Intermittent hypoxia therapy ameliorates beta-amyloid pathology via TFEB-mediated autophagy in murine Alzheimer's disease

Xueting Wang^{1*†}, Yuqi Xie^{1†}, Guijuan Chen¹, Yapeng Lu¹, Dan Wang¹ and Li Zhu^{1*}

Abstract

Background Alzheimer's disease (AD) is the most prevalent neurodegenerative disorder. Impaired autophagy in plaque-associated microglia (PAM) has been reported to accelerate amyloid plaque deposition and cognitive impairment in AD pathogenesis. Recent evidence suggests that the transcription factor EB (TFEB)-mediated activation of the autophagy–lysosomal pathway is a promising treatment approach for AD. Moreover, the complementary therapy of intermittent hypoxia therapy (IHT) has been shown to upregulate autophagy and impart beneficial effects in patients with AD. However, the effect of IHT on PAM remains unknown.

Methods 8-Month-old APP/PS1 mice were treated with IHT for 28 days. Spatial learning memory capacity and anxiety in mice were investigated. AD pathology was determined by the quantity of nerve fibers and synapses density, numbers of microglia and neurons, A β plaque deposition, pro-inflammatory factors, and the content of A β in the brain. TFEB-mediated autophagy was determined by western blot and qRT-PCR. Primary microglia were treated with oligomeric A β 1–42 (oA β) combined with IHT for mechanism exploration. Differential genes were screened by RNA-seq. Autophagic degradation process of intracellular oA β was traced by immunofluorescence.

Results In this study, we found that IHT ameliorated cognitive function by attenuating neuronal loss and axonal injury in an AD animal model (APP/PS1 mice) with beta-amyloid (A β) pathology. In addition, IHT-mediated neuronal protection was associated with reduced A β accumulation and plaque formation. Using an in vitro PAM model, we further confirmed that IHT upregulated autophagy-related proteins, thereby promoting the A β autophagic degradation by PAM. Mechanistically, IHT facilitated the nuclear localization of TFEB in PAM, with TFEB activity showing a positive correlation with A β degradation by PAM in vivo and in vitro. In addition, IHT-induced TFEB activation was associated with the inhibition of the AKT–MAPK–mTOR pathway.

Conclusions These results suggest that IHT alleviates neuronal damage and neuroinflammation via the upregulation of TFEB-dependent A β clearance by PAM, leading to improved learning and memory in AD mice. Therefore, IHT may be a promising non-pharmacologic therapy in complementary medicine against AD.

Keywords Alzheimer's disease, Transcription factor EB, Plaque-associated microglia, Beta-amyloid degradation, Autophagy

[†]Xueting Wang and Yuqi Xie have contributed equally to this work.

*Correspondence:

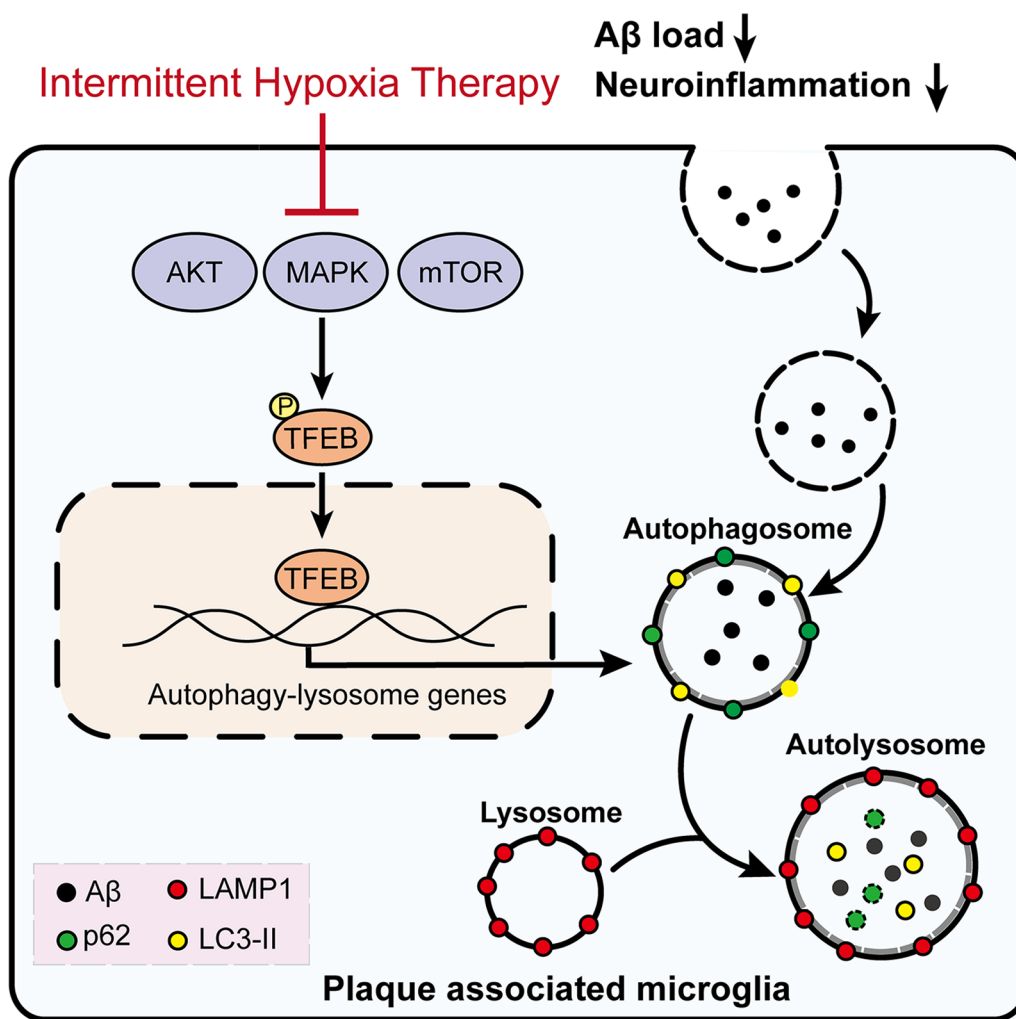
Xueting Wang
wangxueting@ntu.edu.cn

Li Zhu
zhulizhou@ntu.edu.cn

Full list of author information is available at the end of the article



Graphical Abstract

**Introduction**

Alzheimer's disease (AD), which is the most common neurodegenerative disease, is characterized by two major pathological brain lesions, i.e., amyloid plaques (composed mainly of beta-amyloid [A β]) and neurofibrillary tangles (primarily comprising hyperphosphorylated tau). The accumulation and aggregation of A β and tau are detrimental to neurons, eventually leading to neurodegeneration. Therefore, stimulating the clearance of these neuropathological aggregates is an attractive therapeutic strategy for AD [1, 2]. Moreover, A β is suggested to drive tau pathology, with the lowering of A β to certain levels showing beneficial effects in clinical treatment [3]. However, no effective medication currently exists for AD. Nevertheless, drugs such as aducanumab Aduhelm

(approved by the United States Food and Drug Administration in 2021) have been demonstrated to reduce A β plaques [4]; however, their effectiveness and safety remain unclear [5].

Accumulating evidence suggests that the phagocytic and degradative activities of microglia are crucial in eliminating A β from the brain [6–8]. Amyloid precursor protein is processed into A β monomers by β/γ -secretases in neurons. A β monomers are the most abundant form in the brain and forms A β oligomers (oA β s) and fibrillar A β , which further lead to the formation of amyloid plaques. Among these three types of A β , oA β is considered the most neurotoxic form, causing glial cell activation and neuroinflammation [9]. In early stage AD, oA β s enhance A β autophagic

degradation by upregulating LC3-associated endocytosis (LANDO) in microglia [10]. These α A β s are then internalized by microglia via the receptor TREM2 and degraded in the autolysosomes [11]. Thus, LANDO is a key process in maintaining A β homeostasis in the brain.

In late-stage AD, plaque-associated microglia (PAM) show markedly impaired autophagic function, resulting in exacerbated plaque deposition and cognitive damage [12–14]. In particular, PAM primarily uses the autophagy–lysosomal pathway (ALP) for A β degradation, wherein the transcription factor EB (TFEB) is the main regulator [15, 16]. TFEB is a transcriptional autophagy regulator activated by dephosphorylation and nuclear translocation, a process inhibited by signaling kinases, such as mTOR, MAPK, and AKT [17]. TFEB activation by oxidative stress induces autophagy upregulation, which in turn confers neuroprotection, thus making it a potential therapeutic target. [18]. Moreover, increasing research suggests that TFEB activation enhances microglia-mediated clearance of A β plaques, thereby improving cognitive function via autophagy upregulation in the brains of AD animals [19–21]. Therefore, targeting TFEB activation appears to be an effective AD therapy.

Intermittent hypoxia therapy (IHT) improves an organism's physiological and biochemical adaptations to hypoxia by inducing intermittent moderate hypoxia in the organism. Clinical studies have found that IHT boosts exercise tolerance in patients with chronic cardiovascular disease, chronic obstructive pulmonary disease, or metabolic disease [22]. These IHT benefits may be associated with optimizing mitochondrial metabolism and preventing reactive oxygen species (ROS) production [23]. Specifically, IHT upregulates autophagy through the mTOR pathway, leading to enhanced neuroplasticity, reduced myocardial ischemic injury, improved vascular endothelial function, and decreased endoplasmic reticulum stress and apoptosis [24, 25]. In line with these findings, Schega et al. observed that IHT positively affected cognitive function in a study of an older population [26].

Studies have reported that IHT ameliorates certain diseases by activating the autophagy pathway [24, 25]. Song et al. showed that IHT resisted apoptosis in pancreatic β -cells by inducing autophagy and activating the endoplasmic reticulum stress-related PERK/eIF2 α /ATF4 pathway [27]. Chi et al. showed that IHT administered to rats at 8 h per day for a total of 35 days ameliorates myocardial injury by upregulating autophagy [28]. IHT is known to induce the protective oxidative response of cells, with mild oxidative stress being shown to be neuroprotective via the induction of TFEB-mediated autophagy [18, 25, 29]. TFEB, a main transcription factor regulating the ALP [15, 19, 30], enhances A β clearance by PAM [19,

31]. Thus, we hypothesize that IHT has the potential to improve autophagy by upregulating lysosomal function.

Recent studies have revealed that IHT provides superior protection against AD by reducing brain A β deposition and alleviating cognitive function [32, 33], indicating that IHT is a promising strategy for symptomatic AD treatment. Therefore, elucidating the underlying mechanism of IHT in ameliorating AD to promote the clinical use of IHT in AD treatment is crucial. Here, we found that IHT improved PAM function by activating TFEB, resulting in enhanced A β autophagic clearance and consequently reduced neural damage and improved cognitive function in AD models.

Materials and methods

Animals and treatments

Specific pathogen-free (SPF), male APP/PS1 (B6C3-Tg [APP^{swe}, PSEN1^{de9}] 85Dbo/J [005864]) and wild-type littermate control C57BL/6 J mice on a C57BL/6J background aged 6–8 months were purchased from Nanjing Junke Bioengineering Corporation, Ltd. (Nanjing, China; certification number SCXK 2020-0009). Animals were maintained at 23 ± 2 °C under 45–60% humidity and a standard 12/12-h light/dark cycle. For TFEB activation, 6-month-old mice were orally administered TFEB activator 1 (TA1, 10 mg/kg/day; MedChemExpress, HY-135825, CAS: 39777-61-2) or vehicle (corn oil) for 3 months [31]. During IHT, mice were placed in a 60 cm \times 30 cm \times 25 cm chamber with rapidly adjustable oxygen levels. In this therapy, the oxygen concentration in the chamber was initially reduced to 8% within 30 s and maintained for 8 min by introducing compressed nitrogen, followed by compressed oxygen to restore the oxygen concentration to 21% within 30 s and sustained for 8 min. A total of 10 cycles of this hypoxia–normoxia exposure was performed daily for 28 days between 09:00 and 11:00. The IHT protocol was modified from a procedure that has proven to be neuroprotective in $5 \times$ FAD mice [33]. After IHT, the mice were euthanized and perfused with 0.9% saline via the left ventricle to remove the blood.

Morris water maze (MWM) test

MWM tests for spatial learning-memory behavior were conducted as previously described by Zha et al. [34]. The maze was divided into four equal quadrants: the northeast, southeast, southwest, and northwest. Visual cues were posted on the laboratory walls around the maze to facilitate the spatial learning of the platform's location. After IHT, mice were placed in a 150-cm circular pool with water temperature maintained at 21 ± 1 °C. A circular escape platform (10 cm in diameter) was placed in the middle of the southwest quadrant at 1.5 cm below the water surface. The water was made opaque with a

non-toxic, white pigment. The mice were allotted 60 s to locate the platform and were allowed to stay on it for 20 s. The mice were trained four times per day for 5 days. On the 6th day, the hidden platform was removed from the destination quadrant. The mice were then released in the northeast quadrant and allowed to swim freely for 60 s. Video recordings were used to analyze and record the swimming trajectory of each mouse, along with measurement of the time required by the mice to initially find the escape platform, time spent in the target quadrant, and the average swimming speed.

Open field test (OFT)

The OFT was used to assess the anxious behavior of the mice and was performed according to a prior study by Kraeuter et al. [35]. After IHT treatment, the mice were individually placed in a white polyvinyl chloride box (40 cm × 40 cm × 40 cm) and allowed to move freely for 5 min. An overhead camera was used to capture the movement of the test animal in the peripheral (15 cm from the wall) and central zones (25 cm × 25 cm). The number of entries and time spent in the central area by the mice were also recorded.

Elevated plus maze (EPM) test

The EPM test was employed to measure anxiety-related behavior in the mice and was conducted as previously described [36]. Briefly, the mice were positioned at the junction of the four arms (two open and two closed arms) of a maze (35 cm × 5 cm, 50 cm from the ground) facing an open arm and allowed to freely explore the maze for 5 min. Their behavior was recorded using a video camera above the maze. In addition, the entries and time spent by the mice in the open and closed arms were recorded.

Nissl staining

Brain sections (30 μm) of the euthanized mice were fixed using 4% neutral paraformaldehyde and stained with 1% tar violet. The samples were subsequently dehydrated using an ethanol gradient and transparent xylene. The samples were imaged using a Leica DM4000B microscope.

Primary microglia culture and IHT for the microglia

Primary microglia culture Based on previously described protocols [37–39], primary microglial cells were obtained from the cerebral cortices of 3-day-old C57BL/6 mice. After removing the meninges, cortical tissue was digested using 0.05% trypsin. The separated cells were then cultured in Dulbecco's modified Eagle's medium-F12 supplemented with 10% fetal bovine serum, 5 ng/ml of Granulocyte–macrophage colony-stimulating factor (STEMCELL Technologies, 78017), and penicillin/

streptomycin (100 U/ml and 100 mg/ml, respectively) at 37 °C in a 5% CO₂ humidified incubator. After 10 days, the mixed cell population was dominated by astrocytes and formed a fused trophoblast. The microglia gradually proliferated and floated in the supernatant. Finally, the cells from the supernatant were harvested and seeded in 35-mm confocal dishes.

IHT for the primary microglial cells The cell cultures were placed in the same intermittent hypoxia chamber used for the experimental mice. The cells were exposed to 21% oxygen (8 min) and 8% oxygen (8 min) for 10 cycles.

Construction of the in vitro PAM model

Lyophilized Aβ_{1–42} (Anaspec, AS-20276) were dissolved in PBS and incubated overnight at 4 °C to form oligomers (oAβ) [40]. The microglial cells were treated with 1 μM of oAβ for 0, 3, 6, 9, 12, 18, and 24 h. The residual oAβ in the supernatant was detected via ELISA to evaluate the ability of the microglia to metabolize oAβ. Phagocytosis ability and autophagy flux were determined as described below.

TA1 treatment

TA1 (CAS 39777-61-2) purchased from MedChem-Express (HY-135825, 99.69% purity) was dissolved in DMSO to yield a final concentration of 25 mg/ml. It was further diluted tenfold to 2.5 mg/ml with corn oil for animal treatment. In the case of the mice treatment, 6-month-old APP/PS1 mice were administered TA1 orally at 10 mg/kg for 3 months. For cell treatment, TA1 was further diluted to 1 mM in DMSO and directly added to the culture medium to produce a working concentration of 1 μM.

Bafilomycin A1 treatment

Bafilomycin A1 (CAS 88899-55-2) was procured from MedChemExpress (HY-100558, 98.77% purity). The colocalization of Aβ and LAMP1 in PAM in vitro was examined by adding 100 nM of bafilomycin A1 to the culture medium at 1 h before cell fixation.

Detection of the activation of TFEB pathway

TFEB pathway activation were determined by transcriptome screening and qRT-PCR validation. After IHT treatment, total RNA was isolated with TRIzol reagent. The purified total RNA was then submitted to Gene Denovo Biotechnology Co. for RNA-seq. Furthermore, purified total RNA was reverse-transcribed using the HiScript III 1st Strand cDNA Synthesis Kit (Vazyme Biotech, R312-02), according to the manufacturer's instructions and qRT-PCR was performed via the AceQ qPCR SYBR Green Master Mix (Vazyme Biotech, Q141-02).

To further confirm the relationship between IHT and TFEB, primary microglia were transfected by lentivirus expressing mouse *shTfeb* (#1, #2 and #3) to silence TFEB expression. A β -555 endocytosis and degradation, and autophagy level were determined.

Lentivirus transfection

After 70% fusion of the trophoblast cells (approximately 7 days of primary culture), the cells were incubated with 8×10^7 TU of lentiviruses per 25 cm² culture flask and allowed to grow until microglia production. The lentivirus transfection efficiency was approximately 70% in the harvested microglia. Lentivirus expressing LC3-GFP was used to observe autophagosomes. In addition, lentivirus expressing mouse *shTfeb* (#1 target sequence: CGGCAG TACTATGACTATGAT, 2# target sequence: GCGGCA GAAGAAAGACAATCA, and #3 target sequence: GGA GATGACTAACAAGCAGCT) was used to silence TFEB expression.

A β -555 endocytosis and degradation assay

Confocal imaging Primary microglial cells were incubated with 1 μ g/ml of oligomer A β 1–42, HiLyte™ Fluor 555 (A β -555) (Anaspec, AS-60480-01) for 30 min, followed by fixation with 4% paraformaldehyde for endocytosis analysis. In the degradation assay, the microglia were further chased with fresh medium and incubated for 30 min, followed by immediate fixation with 4% paraformaldehyde. Finally, the microglial cells were counterstained with DAPI, and confocal imaging was performed (552 nm; Leica SP8). Positive signals within a single cell were estimated using FIJI Image J (National Institutes of Health).

Flow cytometry The harvested microglial cells were incubated directly with A β -555 for 30 min. The ratio of positive cells containing the HiLyte 555 signal was determined using flow cytometry.

Immunofluorescence staining

Tissue sections (40 μ m) and cultured cells were fixed with 4% paraformaldehyde. The samples were subsequently permeabilized with 0.5% Triton X-100. The samples were then blocked in 10% donkey serum, followed by incubation with the following antibodies: anti-MAP2 (Sigma-Aldrich, M4403), anti-A β 1–16 (BioLegend, SIG-39300), anti-Iba1 (Abcam, ab5076), anti-TFEB (Proteintech, 13372-1-AP), anti-LC3A/B (Cell Signaling Technology, 12741S), anti-LAMP1 (Abcam, ab24170), and anti-synaptophysin (Cell Signaling Technology, 9020). The binding of the primary antibodies was visualized using Alexa Fluor 555-conjugated donkey anti-rabbit IgG (Thermo Fisher Scientific, A31572), Alexa Fluor 488-conjugated donkey anti-mouse IgG (Thermo Fisher Scientific,

A21202), or Alexa Fluor 647-conjugated donkey anti-goat IgG (Abcam, ab150131). Finally, the samples were counterstained with DAPI, and confocal microscopy (Leica Thunder or Leica SP8 confocal microscope) was used to capture the fluorescence images.

RNA isolation and qRT-PCR

Total RNA from the samples was isolated with a TRIzol reagent. Purified total RNA was reverse-transcribed using the HiScript III 1st Strand cDNA Synthesis Kit (Vazyme Biotech, R312-02), according to the manufacturer's instructions. The purified total RNA was then submitted to Gene Denovo Biotechnology Co. for RNA-seq. Furthermore, qRT-PCR was performed via the AceQ qPCR SYBR Green Master Mix (Vazyme Biotech, Q141-02).

All primers used for qRT-PCR were designed as follows.

Lamp1, forward: 5'-CAGCACTCTTTGAGGTGA AAAAC-3', reverse: 5'-ACGATCTGAGAACCATTC GCA-3'.

Il1b, forward: 5'-TGCCACCTTTTGACAGTGATG-3', reverse: 5'-TGATGTGCTGCTGCGAGATT-3'.

Tnf, forward: 5'-AAGCCTGTAGCCCACGTCGTA-3', reverse: 5'-GGCACCCTAGTTGGTTGTCTTTG-3'.

Tgfb, forward: 5'-TGATACGCCTGAGTGGCTGTCT-3', reverse: 5'-CACAAGAGCAGTGAGCGCTGAA-3'.

Wipi2, forward: 5'-TGCTGGTAGGAGCATCAG ATGG-3', reverse: 5'-TCACTGGTCGTCTCCATA CTGC-3'.

Vps11, forward: 5'-ATCGGCAGTCTCTGGCTA ATGC-3', reverse: 5'-GGACCTTGATGGCTGTCT CTAC-3'.

Vps18, forward: 5'-AAGTGAGCCCAACCGTGT GGAA-3', reverse: 5'-AAAGGACCTCGGTGCTAC TCAG-3'.

Actb, forward: 5'-CATCCGTAAAGACCTCTATGC CAAC-3', reverse: 5'-ATGGAGCCACCGATCCAC A-3'.

The relative amount of gene expression was calculated using Δ Ct values, where Ct represents the threshold cycle of PCR.

Estimation of A β 1–42 and A β 1–40 levels

Soluble and insoluble proteins from the mice brains, supernatant, or cultured microglia were diluted to 21% using PBS to determine A β 1–42 and A β 1–40 levels via specific ELISA methods. The test procedures were performed according to the manufacturer's instructions for the Human A β 1–40 ELISA Kit (Immunoway Biotechnology, KE1389) and Human A β 1–42 ELISA Kit (Immunoway Biotechnology, KE1390). The optical density was

measured at 450 nm. In addition, the standard curve was created using a four-parameter logistic curve fit with Origin 8.0 software (<https://www.originlab.com>).

Protein isolation and western blot

The samples were lysed in RIPA buffer to obtain soluble proteins. The precipitates were further cleaved with RIPA buffer containing SDS and urea to obtain insoluble proteins. The protein concentration was determined via bicinchoninic acid assay. The proteins were then isolated and transferred to polyvinylidene fluoride membranes. Next, the membranes were incubated with primary antibodies, including anti-A β 1–16 (BioLegend, SIG-39300), anti-TFEB (Proteintech, 13372-1-AP), anti-phospho-MAPK (Cell Signaling Technology, 4370), MAPK (Cell Signaling Technology, 4695), anti-p-Akt (Cell Signaling Technology, 4060 T), anti-Akt (Cell Signaling Technology, 4685 s), anti-ribosomal protein S6 (RPS6; Santa Cruz Biotechnology, sc-74459), anti-p-RPS6 (Cell Signaling Technology, 2211), anti-mTOR (Santa Cruz Biotechnology, sc-517464), anti-p-mTOR (Santa Cruz Biotechnology, sc-293133), anti-p62 (Proteintech, 18420-1-AP), anti-LC3A/B (Cell Signaling Technology, 12741S), anti-LAMP1 ([Santa Cruz Biotechnology, sc-20011] or [Abcam, ab24170]), and anti- β -actin (Sigma-Aldrich, A5316). The binding of the primary antibodies was visualized using HRP-conjugated secondary antibodies. Furthermore, grayscale analysis was conducted using FIJI ImageJ (National Institutes of Health).

Statistical analysis

GraphPad Prism version 8 (GraphPad) was used to analyze the data. A Student's *t* test and one- or two-way ANOVA followed by Dunnett's multiple comparisons were applied for statistical assessment. Data are presented as mean \pm Standard Error of Measurement (SEM). The significance levels for all the graphs were as follows: * $P < 0.05$, ** $P < 0.01$, and *** $P < 0.001$. *P* values with no statistical difference have been marked in the graph.

Results

IHT ameliorates cognitive function in APP/PS1 mice

We administered IHT (8% O₂ for 8 min and 21% O₂ for 8 min, 10 cycles/day) in 8-month-old APP/PS1 and wild-type (WT) littermate control mice for 28 days (Fig. 1A). The Morris water maze (MWM) results revealed that the swimming trajectories to reach the platform in the training trials were longer in the APP/PS1 mice than in the WT mice, while IHT-treated APP/PS1 mice demonstrated a shorter swimming route to the target quadrant (Fig. 1B). In the probe trials, the WT mice remained in the target quadrant, whereas the APP/PS1 mice exhibited indiscriminate movement to all quadrants. In contrast, the IHT-treated APP/PS1 mice displayed extended dwelling in the target quadrant (Fig. 1D). Furthermore, the latency to reach the escape platform for the first time was significantly longer in the APP/PS1 mice than in the WT mice, whereas IHT significantly shortened the latency time in the APP/PS1 mice during the 5-day training duration (Fig. 1C). Consistent with these findings, the results of the probe trials on the 6th day showed that the APP/PS1 mice had a shorter dwelling time in the target quadrant and a longer latency time than the WT mice, and these values were largely reversed by IHT (Fig. 1D, E). However, the swimming speed was similar across all mice groups, suggesting that IHT has little effect on the muscle (Fig. 1F). Moreover, the open field and elevated plus maze tests indicated that IHT did not improve the anxiety of the mice (Additional file 1: Fig. S1). All these results suggest that the learning and memory of 8-month-old APP/PS1 mice were significantly impaired and that IHT effectively improved the cognitive function of these mice.

We further investigated whether the behavioral improvement of the IHT-treated APP/PS1 mice was associated with changes in their neural structures. Our examination showed a significant loss of axons and dendrites in the brain of the APP/PS1 mice. Furthermore, IHT significantly blocked this neuronal loss

(See figure on next page.)

Fig. 1 IHT improves learning and memory and ameliorates neural damage in APP/PS1 mice. **A** Design of the IHT system is illustrated. In the IHT procedure, 8-month-old APP/PS1 and wild-type littermate control mice were treated with 10 alternating cycles of 21% O₂ (8 min) and 8% O₂ (8 min) daily (160 min/day) for 28 days. **B** After IHT, the mice were trained in the MWM for 5 consecutive days. The mice swimming trajectories in the water maze on the 5th day (training test) and on the 6th day after the escape platform was removed (probe test) were recorded. **C** Latencies to reach the escape platform from the contralateral quadrant were recorded during the continuous 5-day training. **D** In the probe test, the dwelling time in the target quadrant was calculated as the percentage of the total time. **E** During the probe test, the latency to reach the target quadrant for the first time was recorded. **F** In the probe test, the average swimming speed was obtained by calculating the total swimming distance divided by the total duration. **G** Axonal labeling in the brain sections of the IHT-administered mice was performed by staining with anti-MAP2 antibodies. Scale bar = 50 μ m. **H** Axonal integrity was determined by calculating the relative area of MAP2 signals in the hippocampal CA1 and CA3 regions and the cortex. **I** Neurons in the brain sections were labeled with Nissl staining. Scale bar = 100 μ m. **J** Number of neurons in the hippocampal CA1 and CA3 region and the cortex was estimated by counting the blue particles. $n = 7$ in panels C–F; $n = 4$ in panels H–J. * $P < 0.05$, ** $P < 0.01$, and *** $P < 0.001$ by two-way ANOVA. *Ctx* cortex, *Hipp* hippocampus, *TG* APP/PS1 transgenic mice

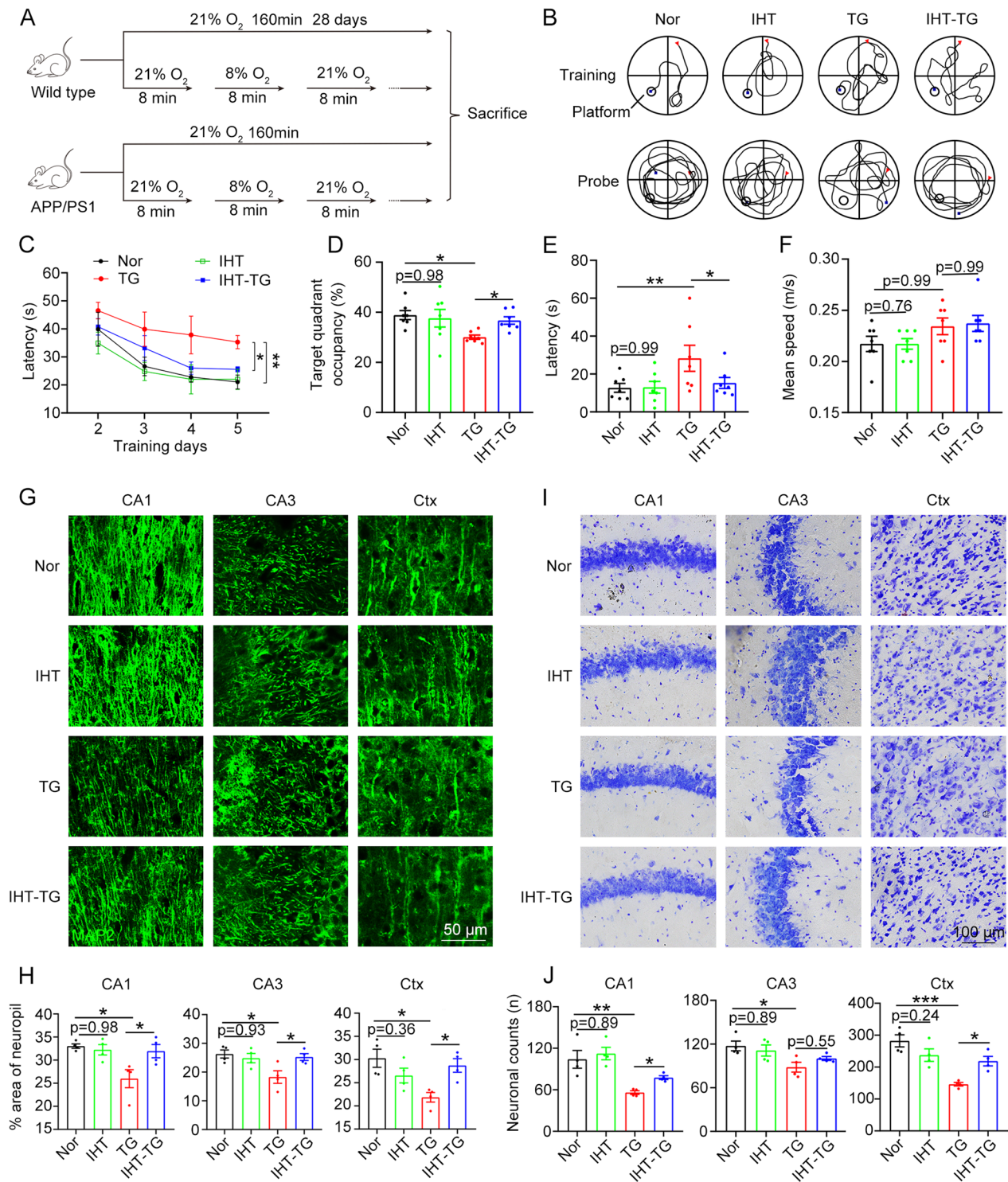


Fig. 1 (See legend on previous page.)

in the hippocampal CA1 and CA3 and cortical regions of the APP/PS1 mice (Fig. 1G, H, Additional file 1: Fig. S2). In addition, compared with the WT mice, the APP/PS1 mice exhibited a significantly reduced number of

brain neurons, which was reversed after IHT (Fig. 1I, J). Considering these findings, IHT may improve cognitive function by mitigating neuronal impairment in APP/PS1 mice.

IHT alleviates A β pathology and neuroinflammation in APP/PS1 mice

To further confirm whether IHT-induced cognitive function improvement in the APP/PS1 mice was related to changes in A β pathology, we co-labeled A β plaques with the microglial marker Iba1 in mouse brain sections (Fig. 2A). Our findings revealed that IHT significantly reduced the number and area of A β plaques in the cortex and hippocampus (Fig. 2B–D), which was accompanied by fewer activated microglia (Fig. 2E). Furthermore, IHT significantly reduced the levels of A β 1–40 and A β 1–42

(Fig. 2F, G), the most common A β subtypes, suggesting that IHT effectively suppresses A β plaque deposition.

We additionally explored the effect of IHT on A β clearance by PAM. As demonstrated in Fig. 2H, I, IHT significantly upregulated lysosome formation in PAM, along with significantly increasing the colocalization of the lysosomes with A β (Fig. 2J), suggesting that IHT promotes the lysosomal clearance of A β in PAM. Furthermore, IHT alleviated neuroinflammation in the APP/PS1 mice, as evidenced by the reduced levels of pro-inflammatory factors IL-1 β and TNF- α and upregulated anti-inflammatory

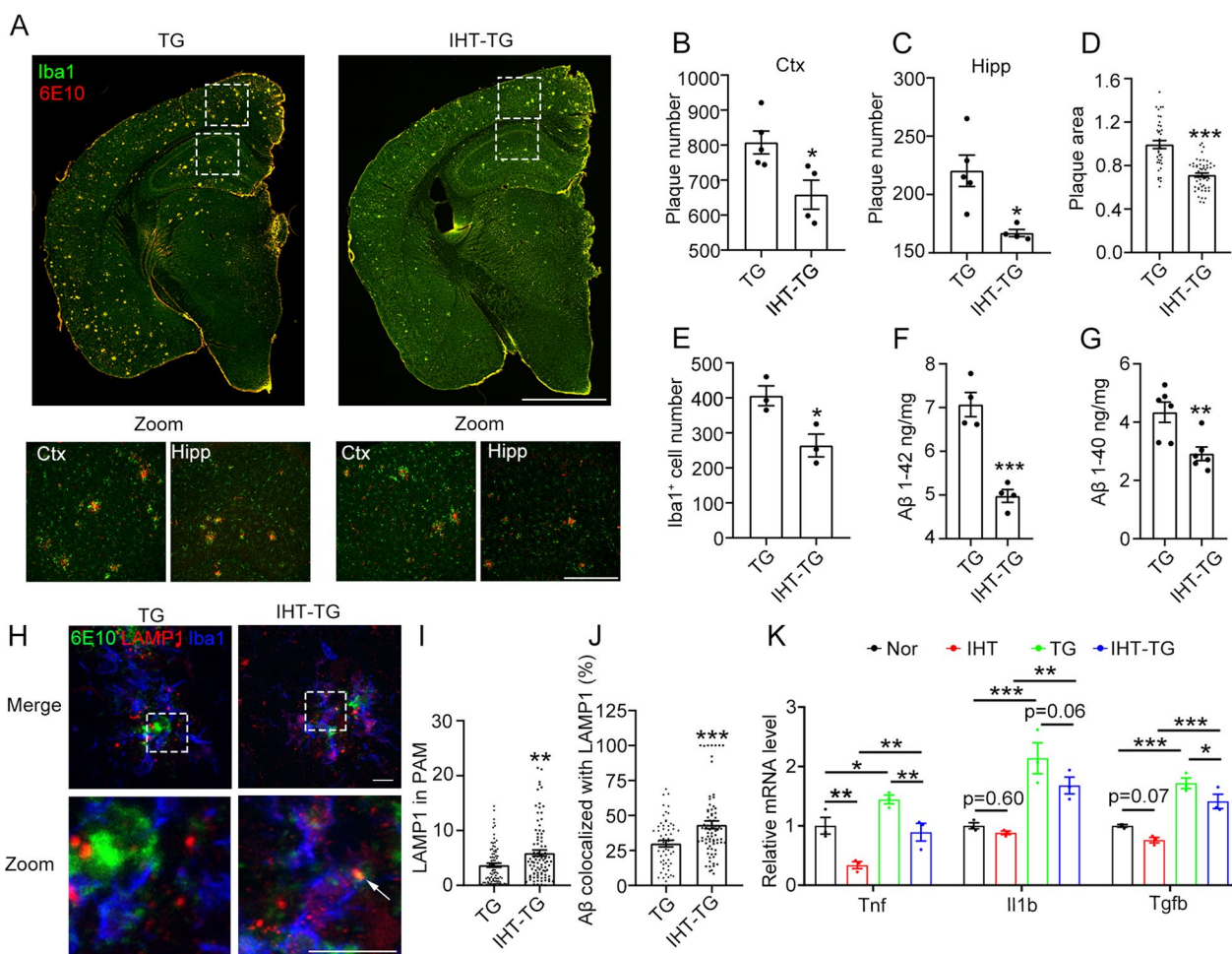


Fig. 2 IHT reduces plaque accumulation, enhances A β degradation, and attenuates the expression of pro-inflammatory factors. During IHT, 8-month-old APP/PS1 mice underwent IHT for 28 days. **A** Mice brain sections were probed with anti-A β 1–16 (6E10) and anti-Iba1 antibodies to detect A β plaques and microglia. The cortex and CA1 region of the hippocampus are circled and zoomed in. Scale bar = 2 mm or 300 μ m. **B, C** Total of 12 evenly spaced brain slices were acquired from each mouse, and the number of plaques in the hippocampus and cortex was quantified by counting the 6E10 signals. $n = 5$. **D** Plaque area was obtained by measuring the average area of the 6E10 signals. $n > 40$. **E** Microglia number was estimated by counting all Iba1 $^{+}$ cells in the hemispheres. $n = 3$. **F, G** A β 1–42 and A β 1–40 concentrations in the brain tissues were determined via ELISA. $n = 4$ and 6. **H** Brain sections were co-stained with anti-LAMP1, anti-Iba1, and anti-A β 1–16 (6E10) antibodies to observe the degraded A β in PAM. Scale bar = 10 μ m. **I** LAMP1 in PAM were calculated by measuring the mean intensity of LAMP1 in Iba1 $^{+}$ 6E10 $^{+}$ cells. $n > 90$. **J** Colocalization ratio of A β with LAMP1 in Iba1 $^{+}$ cells were determined using Manders' colocalization coefficients. $n > 50$. **K** mRNA levels of *Il1b*, *Tnfa*, and *Tgfb* in the hippocampus were obtained via qRT-PCR. $n = 4$. * $P < 0.05$, ** $P < 0.01$, and *** $P < 0.001$ using Student's *t* test. *Ctx* cortex, *Hipp* hippocampus, *TG* APP/PS1 transgenic mice

factor TGF- β (Fig. 2K). Therefore, IHT enhances A β clearance by PAM and reduces A β plaque accumulation and neuroinflammation.

IHT-stimulated A β clearance is accompanied by autophagy activation in PAM

We hypothesized that the effect of IHT on AD pathology is mediated by the upregulation of the ALP. After IHT, lysosomal-associated membrane protein 1 (LAMP1) and LC3I/II levels in the hippocampus of APP/PS1 mice were significantly upregulated and that of the insoluble content of the autophagy substrate SQSTM1/p62 was decreased, suggesting that IHT upregulates the ALP (Fig. 3A, B). Moreover, considering that A β clearance in the brain depends primarily on microglial autophagy [6], we further examined the effects of IHT on autophagosome formation in PAM. As shown in Fig. 3C, and D, the punctate intensities of LC3 (a well-known autophagosome marker) increased significantly in PAM after IHT. The colocalization of LC3 with LAMP1 was also increased in PAM, suggesting enhanced autolysosome formation (Fig. 3C, E). Consistent with the autophagy-dependent degradation of A β in PAM, elevated A β levels and increased colocalization of A β with LC3 were observed in PAM after IHT (Fig. 3F–H). These findings suggest that IHT enhances A β clearance by stimulating the ALP in PAM.

To further validate that IHT modulates its effects via microglia, an *in vitro* PAM model was established to enable the direct exposure of microglia to prolonged oA β activation. As shown in Fig. 3I, microglia quickly degraded oA β in the medium within 3 h of oA β exposure, but the subsequent clearance activity was significantly diminished, suggesting that prolonged oA β stimulation might impair microglial autophagic degradation of oA β . Furthermore, a single day of IHT treatment (10 cycles of 8% O₂ for 8 min and 21% O₂ for 8 min) dramatically enhanced the clearance of the remaining oA β by the microglia (Fig. 3J). In addition, we observed that the internalization of A β -555 was significantly improved in

the IHT-treated PAM (Fig. 3K, L), wherein IHT was demonstrated to accelerate A β clearance by PAM after 30 min of intracellular degradation, i.e., chase period (Fig. 3M, N). This finding indicates that IHT enhances cellular A β clearance by promoting endocytosis and intracellular A β degradation by PAM. Furthermore, IHT significantly increased the colocalization of A β -555 with LC3 (Fig. 3O, P) and LAMP1 (Fig. 3Q, R), suggesting that IHT can stimulate autophagic degradation of oA β by directly acting on microglia.

IHT upregulates TFEB-mediated autophagy through AKT–MAPK–mTOR signaling

To explore the mechanism by which IHT upregulates oA β degradation in PAM, we screened the PAM cells via RNA sequencing (RNA-seq). As depicted in the heatmap analysis, IHT treatment of PAM *in vitro* significantly increased the expression of ALP-related proteins (Fig. 4A). In addition, the levels of pro-inflammatory factors were decreased and those of anti-inflammatory factors were increased in IHT-treated PAM *in vitro* (Fig. 4A). Similarly, the KEGG pathway analysis revealed that the autophagy and inflammation-related pathways were among the top upregulated pathways (Fig. 4B). In particular, the mRNA levels of autophagy/lysosome-related genes, such as *Lamp1*, *Vps11*, *Wipi2*, and *Vps18*, were upregulated in the IHT-treated PAM *in vitro* (Fig. 4C–F).

Thus, we hypothesized that the IHT-enhanced autophagy was related to TFEB activation. In support of this hypothesis, our *in vitro* and *in vivo* results showed that the nuclear expression of TFEB in PAM was significantly increased after IHT (Fig. 4G–J). Moreover, IHT upregulated the transcription activity of TFEB (Additional file 1: Figs. S3 and S6). In consistent, IHT significantly upregulated the expression of ALP-related genes in mice brains, including *Lamp1*, *Vps11*, *Wipi2*, and *Vps18*, which were also target genes of TFEB (Fig. 4K–N). Next, to address the mechanism of TFEB activation by IHT in

(See figure on next page.)

Fig. 3 IHT enhances autophagy and A β degradation by autophagosomes in PAM *in vivo* and *in vitro*. **A, B** LAMP1, p62, and LC3 in the hippocampus were detected via western blot. $n = 3$ (Student's *t* test). **C–E** Mice brain sections were co-stained with anti-LAMP1, anti-Iba1, and anti-LC3 antibodies. Scale bar = 10 μ m. LC3 accumulation, and colocalization ratio of LC3 with LAMP were quantified in Iba1⁺ cells. $n > 20$ (Student's *t* test). **F–H** Brain sections were co-stained with anti-Iba1, anti-6E10, and anti-LC3 antibodies. Scale bar = 10 μ m. The amount of internalized A β and A β colocalized to LC3 puncta was quantified in Iba1⁺ cells. $n > 40$ (Student's *t* test). **I** Primary microglia were treated with 1 μ M oA β for the indicated durations. A β concentration in the medium was measured using ELISA. $n = 4$ (one-way ANOVA). **J** Primary microglia were treated with 1 μ M oA β for 24 h, followed by a single day of IHT (10 cycles of 21% O₂ and 8% O₂). A β concentration in the medium was determined using ELISA. $n = 7$ (Student's *t* test). **K–N** After oA β and IHT co-treatments, primary microglia were incubated with 1 μ M of A β -555 for 30 min (**K** and **L**), or further washed with fresh medium (Chase) for 30 min (**M** and **N**). Scale bar = 20 μ m. The intracellular A β -555 was quantified using Image J. $n > 40$ (two-way ANOVA). **O–R** Microglia were probed with anti-LC3 or anti LAMP 1 antibodies. Scale bar = 5 μ m. The ratio of A β -555 colocalization with LC3 or LAMP1 in a single cell was determined via Manders' colocalization coefficients. $n > 50$ (two-way ANOVA). * $P < 0.05$, ** $P < 0.01$, and *** $P < 0.001$. IHT intermittent hypoxia therapy, TG APP/PS1 transgenic mice

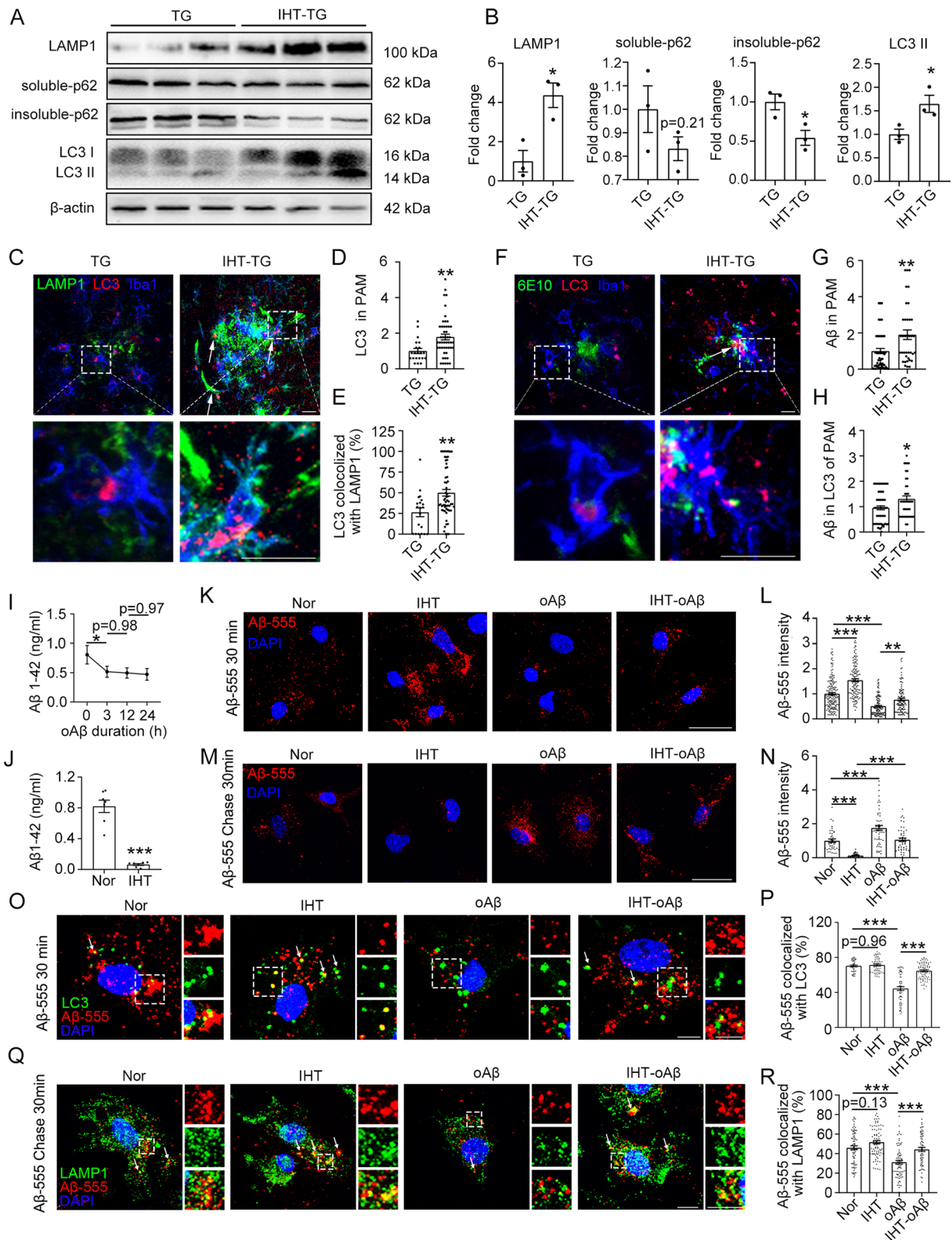


Fig. 3 (See legend on previous page.)

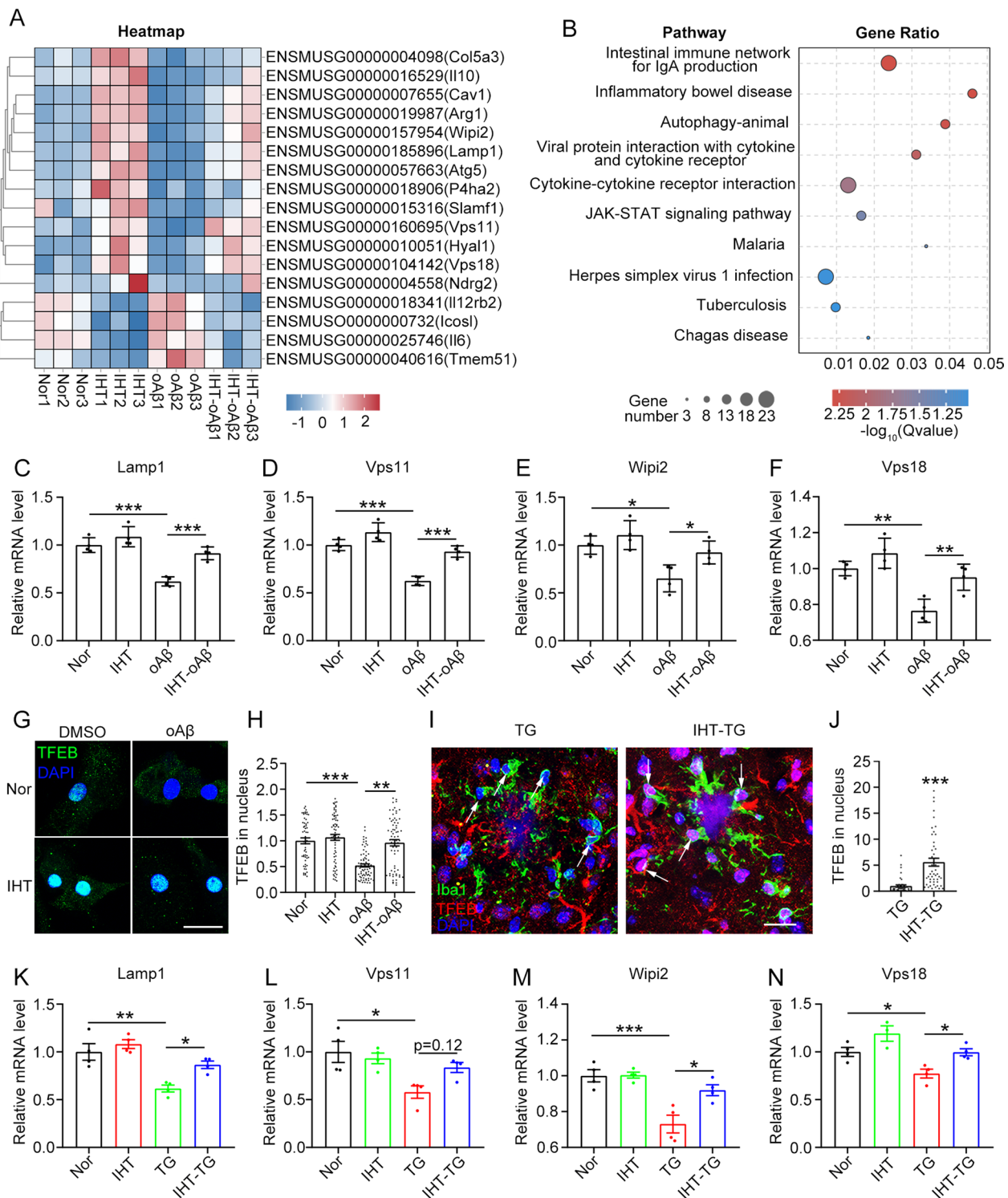


Fig. 4 IHT upregulates the TFEB-related pathway in PAM. **A–F** Total RNA of in vitro PAM was isolated for RNA-seq. Heatmap (**A**) and KEGG pathway (**B**) analyses were used to demonstrate the differentially expressed genes and enriched pathways, respectively. **C–F** Autophagy-related differential genes, including *Lamp1*, *Vps11*, *Wipi2*, and *Vps18*, were detected using qRT-PCR. $n = 3$ (two-way ANOVA). **G, H** In vitro PAM was stained with an anti-TFEB antibody after a single day of IHT. Scale bar = 20 μm . TFEB signals in the microglial nucleus were quantified. $n > 50$ (two-way ANOVA). **I, J** Brain sections of IHT-treated mice were co-stained with anti-Iba1 and anti-TFEB antibodies. Arrows indicate the PAM nucleus. Scale bar = 20 μm . TFEB signals in the PAM nucleus were measured. $n > 50$ (Student's *t* test). **K–N** Autophagy-related genes, such as *Lamp1*, *Vps11*, *Wipi2*, and *Vps18*, in the brains of IHT-treated mice were detected via qRT-PCR. $n = 3$ (two-way ANOVA). * $P < 0.05$, ** $P < 0.01$, and *** $P < 0.001$. TG, APP/PS1 transgenic mice

PAM, we investigated the activities of AKT, MAPK, and mTOR signaling, which serve as the negative regulators of TFEB activation. Our results demonstrated that IHT inhibited the phosphorylation levels of AKT, MAPK, mTOR, and RPS6 in vivo (Additional file 1: Fig. S4A, B) and in vitro (Additional file 1: Fig. S4C, D), indicating that IHT enhanced TFEB activation in PAM by inhibiting AKT–MAPK–mTOR signaling. These results suggest that IHT-enhanced autophagic degradation of A β by PAM is associated with the upregulation of ALP-related proteins, which in turn is mediated by TFEB activation.

TFEB activation ameliorates A β pathology and enhances A β autophagic degradation by PAM in vivo and in vitro

TA1, also named as Curcumin analog C1, was reported as a TFEB-specific activator by binding to the N-terminus of TFEB, promoting TFEB nuclear translocation and activating TFEB-mediated autophagy [41], which has no effect on the pathways regulating autophagy, including mTOR, MAPK1/ERK2 and MAPK3/ERK1. TA1 has been reported to reduce A β pathology and improve cognitive function by effectively activating TFEB in the brain of 3xTg AD model mice [31]. In our study, TA1-induced TFEB nuclear translocation in primary microglial cells (Additional file 1: Fig. S5). Thus, we further examined whether TA1 can alleviate AD pathology by activating the TFEB pathway in the PAM of APP/PS1 mice. Our findings demonstrated that TA1 reduced A β plaques in the mouse brain (Fig. 5A, B) and A β load in the cortex (Fig. 5C). In addition, TA1 increased the transcription activity of TFEB (Additional file 1: Fig. S6) and nuclear translocation of TFEB in PAM (Fig. 5D), which was in line with TA1's established role in TFEB activation [41]. We also revealed that TA1 upregulated the colocalization of A β with LC3 as well as the colocalization of LC3 with LAMP1 in PAM (Fig. 5E–H), consistent with the observation of TFEB-enhanced autophagic degradation of A β .

Furthermore, we examined whether TA1 directly affects microglia. For this purpose, we co-treated microglia with TA1 and oA β . Our results showed that TA1 upregulated the nuclear levels of TFEB (Additional file 1: Fig. S7A, B). In consistent, TA1 upregulated the transcription activity of TFEB (Additional file 1: Fig. S3) and its target genes *Lamp1*, *Vps11*, *Wipi2*, and *Vps18* in PAM in vitro (Additional file 1: Fig. S7C–F). TA1 was also demonstrated to upregulate the colocalization of LC3 with LAMP1 (Fig. 5I, J) and enhance A β clearance by microglia (Fig. 5K), indicating that TFEB activation contributed to oA β degradation. Furthermore, TA1 increased the colocalization ratio of A β -555 with both LC3 and LAMP1 in PAM in vitro (Fig. 5L–O). These findings suggested that TFEB activation by TA1 enhanced A β degradation via the upregulation of the ALP in PAM in vitro, supporting the in vivo results.

IHT enhances TFEB-mediated ALP-dependent A β degradation in microglia

To determine the role of TFEB in the autophagic degradation of A β by microglia, we inhibited TFEB expression by infecting primary microglial cells with lentivirus expressing sh*Tfeb* (#1, #2, and #3) (Fig. 6A). Our results showed that the colocalization of LC3 with LAMP1 was significantly decreased after TFEB silencing (Fig. 6B, C). Furthermore, oA β degradation by microglia was impaired after TFEB knockdown (Fig. 6D), indicating that TFEB is important for A β degradation by microglia.

To further investigate the involvement of TFEB in IHT-enhanced A β degradation by PAM, we silenced TFEB in IHT-treated PAM in vitro. We found that TFEB silencing (Fig. 6F) inhibited the IHT-associated improvement of oA β clearance by microglia (Fig. 6E). Similar to the findings in the primary microglial cells, the absence of TFEB in IHT-treated PAM in vitro prevented the enhanced colocalization of LC3 with LAMP1 (Fig. 6G, H), suggesting that IHT upregulated

(See figure on next page.)

Fig. 5 TA1 enhances the autophagic degradation of A β and reduces A β pathology in APP/PS1 mice. 6-month-old APP/PS1 mice were administered TA1 orally at 10 mg/kg for 3 months. **A, B** Mice brain sections were probed with anti-A β 1–16 (6E10) antibodies. Scale bar = 2 mm. The number of hippocampal and cortical plaques was quantified in twelve evenly spaced brain slices from each mouse. $n = 8, 6$ (Student's *t* test). **C** A β 1–42 in brain tissues was determined using ELISA. $n = 6$ (Student's *t* test). **D** Brain sections were co-stained with anti-TFEB and anti-Iba1 antibodies. Arrows indicate the PAM nuclei. Scale bar = 25 μ m. **E–H** Brain sections were co-stained with anti-LC3, anti-Iba1, and anti-A β 1–16 (6E10) or anti-LAMP1 antibodies. Scale bar = 10 μ m. The colocalization ratio of LC3 with A β or LAMP1 in Iba1⁺ cells were estimated via Manders' colocalization coefficients. $n > 30$ (Student's *t* test). **I, J** Primary microglia were co-treated with oA β and TA1 for 12 h, followed with bafilomycin A1 treatment for 1 h. Then, cells were probed with anti-LC3 and anti-LAMP1 antibodies. Scale bar = 5 μ m. The colocalization ratio of LC3 with LAMP1 in single cell was quantified using Manders' colocalization coefficients. $n > 40$ (two-way ANOVA). **K** A β 1–42 in the medium were then detected using ELISA. $n = 5$ (Student's *t* test). **L–O** After co-treated with oA β and TA1, cells were incubated with A β -555 for 30 min, or co-treated with bafilomycin A1 for 30 min and chased. Then, cells were stained with anti-LC3 or anti-LAMP1 antibodies. Scale bar = 5 μ m. The colocalization ratio of A β -555 with LC3 or LAMP1 was measured via Manders' colocalization coefficients. $n > 50$ (two-way ANOVA). * $P < 0.05$, ** $P < 0.01$, and *** $P < 0.001$. TG, APP/PS1 transgenic mice

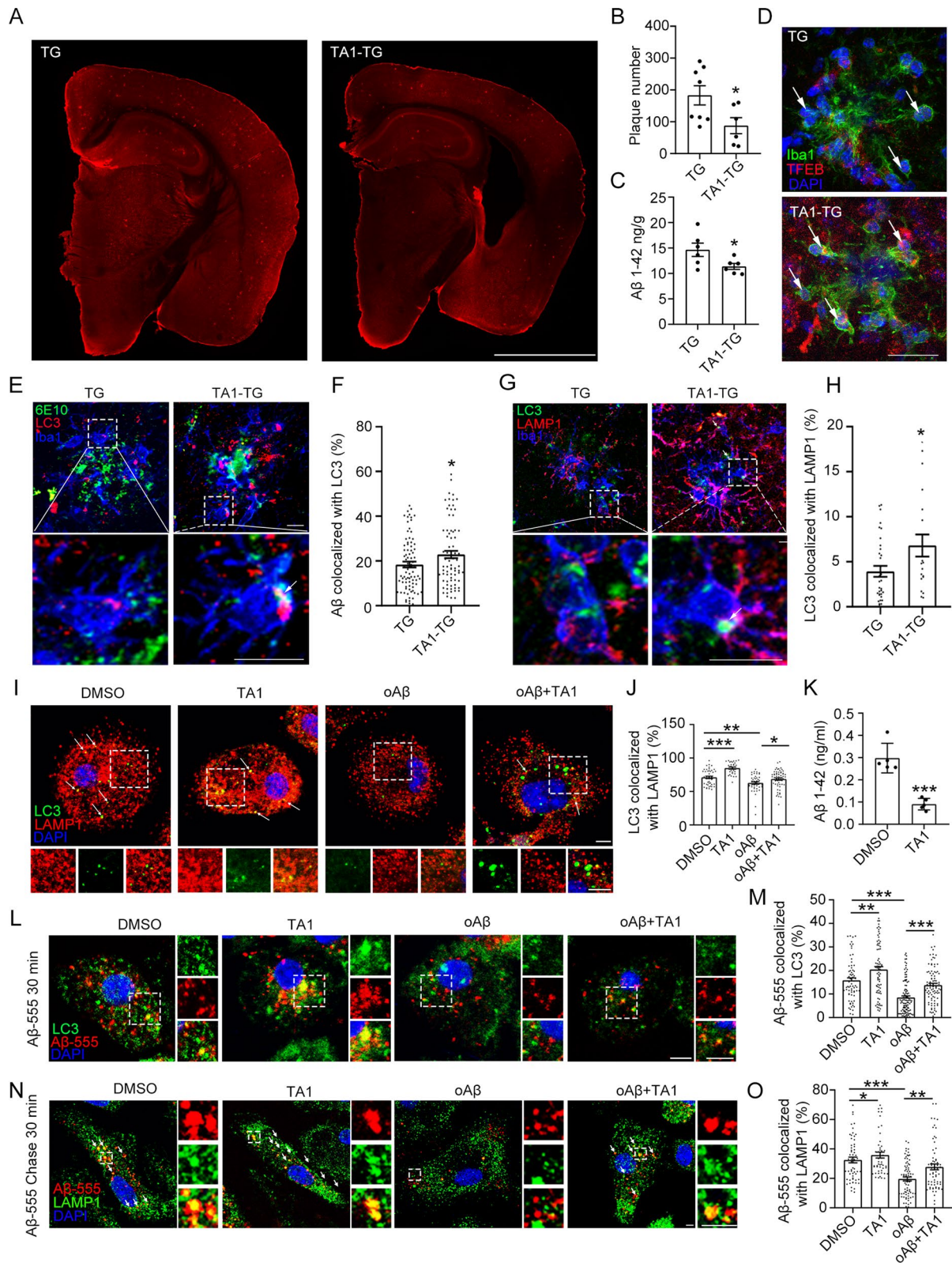


Fig. 5 (See legend on previous page.)

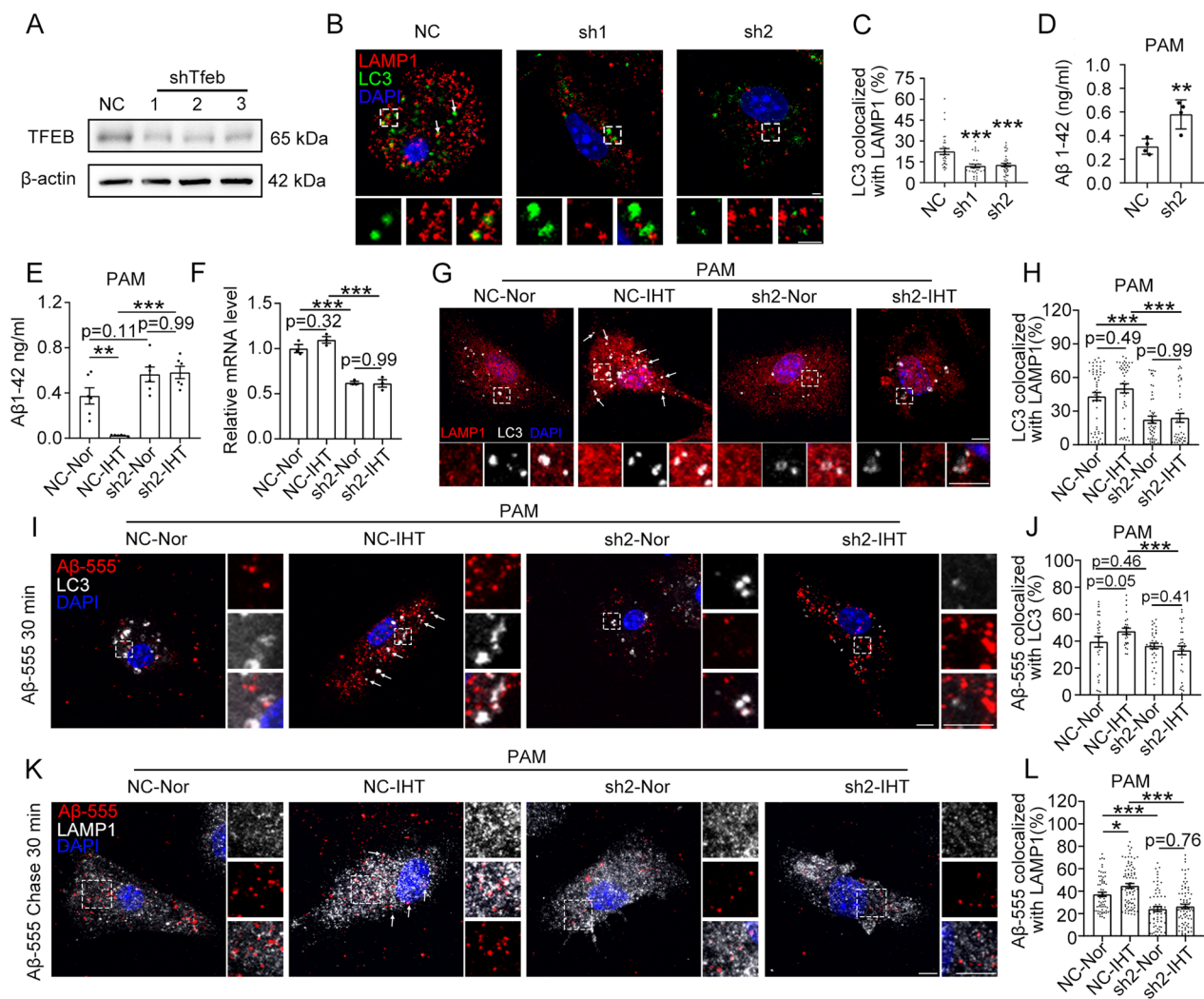


Fig. 6 IHT enhances Aβ degradation by microglia via TFEB-mediated autophagy. **A** Primary microglia were infected with three shTfeb lentivirus (#1, #2, and #3). Interference efficiency were determined by western blot. **B, C** Cells were co-stained with anti-LC3 and anti-LAMP1 antibodies. Scale bar = 5 μm. The colocalization ratio of LC3 and LAMP1 in single cell was quantified using Manders' colocalization coefficients. n > 30 (Student's *t* test). **D** sh-Tfeb #2 lentivirus (sh2)-infected microglia were treated with 1 μM of oAβ for 12 h. Aβ1-42 in the medium were detected with ELISA. n = 4. (Student's *t* test). **E-L** sh-Tfeb #2 lentivirus (sh2)-infected microglia were co-treated with oAβ and a single-day IHT. **E** Aβ1-42 in the medium was measured via ELISA. n = 6. **F** TFEB expression was determined using qRT-PCR. n = 3. **G, H** Cells were treated with bafilomycin A1 for 1 h, followed by staining with anti-LC3 and anti-LAMP1 antibodies. Scale bar = 5 μm. The colocalization ratio of LC3 with LAMP1 was evaluated using Manders' colocalization coefficients. n > 40. **I-L** Cells were treated with Aβ-555 for 30 min, or co-treated with Aβ-555 and bafilomycin A1 for 30 min and chased. Then, cells were stained with anti-LC3 or anti-LAMP1 antibodies. Scale bar = 5 μm. The colocalization ratio of Aβ-555 with LC3 or LAMP1 in a single cell was determined via Manders' colocalization coefficient. n > 30. **P* < 0.05, ***P* < 0.01, and ****P* < 0.001 using two-way ANOVA

the ALP via TFEB. Furthermore, TFEB interference restricted IHT-stimulated augmentation of Aβ-555 colocalization with both LC3 and LAMP1 in PAM in vitro (Fig. 6I–L). Thus, the effect of IHT on the ALP-dependent degradation of Aβ in PAM is mediated by TFEB signaling.

Discussion

Intermittent hypoxia can have contrasting effects on the central nervous system based on the frequency, degree, and duration of hypoxia exposure [42]. Intermittent hypoxic conditions of high intensity, high density, and long periods are known to damage the central nervous

system and are commonly used to simulate sleep apnea [43]. In contrast, intermittent hypoxic stimulation of appropriate intensity exerts a protective effect. Ryou et al. demonstrated that 3 weeks of IHT effectively stabilized neurological function and upregulated neuroprotective trophic factors and erythropoietin in 3xTg-AD model mice, significantly protecting the AD model mice from cognitive impairment [33]. Yue et al. found that IHT with alternately 10 min of 14.3% O₂ and 10 min of 21% O₂, 4 h daily for 14 days, significantly reduced the level of A β plaque and nerve fiber accumulation in the brain of 6-month-old APP/PS1 mice and improve their learning and memory ability [44]. Meng et al. found that IHT with 8 min of 5% O₂ and 8 min 21% O₂ alternately for 4 h every day for 15 days, significantly improved the cognitive impairment of 9-month-old APP/PS1 mice [45]. It was reported that IHT lasting for 28 days or more also showed protective effect. After IHT at an altitude of 7000 m (about 8% O₂) for 8 h per day for 35 days, the infarcted area of the brain reduced and the arrhythmia caused by coronary artery occlusion was improved [46]. Giving 14% O₂ for 12 h a day for 28 days effectively improved the glucose tolerance of diabetic rats [47]. In addition to the hypoxic conditions used in this study, we also treated mice with different levels of intermittent hypoxia, including 5% O₂ for 30 s, 21% O₂ for 30 s with 8 h treatment daily for 28 days, and 12% O₂ for 8 min, 21% O₂ for 8 min with 10 cycles treatment daily for 28 days. We found that the above conditions had no obvious effect on the learning and memory ability of APP/PS1 mice (data not shown), suggesting that the protective effect of IHT on AD mice depends on different hypoxia conditions. The clinical evidence shows that in the past 50 years, IHT with the concentration of 10–15% and the duration of 3 weeks with head-mounted or walk-in equipment produce significant beneficial effects in the treatment of cardiovascular diseases, such as hypertension, coronary heart disease and heart failure [48], proving that IHT has a good prospect in clinic.

In the present study, we found no significant improvement in anxiety by IHT. The relationship between AD and anxiety remains unclear. A study by Hanseeuw et al. showed that, in the early stages of AD, patients did not show anxiety, and in the late stages of AD, anxiety gradually appeared [49]. Zhang et al. demonstrated that Citalopram improved spatial memory and synaptic plasticity in the hippocampus of AD mice, but did not positively affect anxiety-like behavior [50]. Similarly, Xu et al. found that ketogenic diet therapy effectively improved learning cognitive ability and significantly reduced the number of A β plaques and neuroinflammation in the brain, but did not have a significant improvement in anxiety-like behavior [51]. We hypothesized that the improvements

in cognitive functioning would precede the onset of improvements in anxiety.

Our study investigated the modulatory effect of IHT on TFEB-associated autophagy in the PAM of AD mice. Previous literature suggests that the beneficial effects of IHT pretreatment may be related to the optimization of mitochondrial metabolism and the prevention of ROS overproduction [23]. Clinical and basic studies have also revealed that autophagy is significantly reduced in the brains of patients with AD and that A β degradation in the brain mainly depends on autophagic degradation by microglia [10]. Furthermore, impaired phagocytosis and autophagy in PAM were identified as the major factors involved in plaque deposition, neuronal apoptosis, and neuroinflammation in the advanced AD brain [12, 13]. Nevertheless, the reactivation of autophagic activities has shown positive outcomes in AD pathology [52, 53]. In the present study, we determined that IHT effectively stimulated autophagy in PAM and alleviated AD pathology, enhancing the microglial function of clearing A β and reducing A β plaque deposition. Therefore, IHT has promising potential as an adjuvant treatment for AD.

TFEB abnormalities are closely associated with many diseases [15]. Moreover, TFEB is known to promote the transcriptional upregulation of lysosome/autophagy genes by directly binding to the Coordinated Lysosomal Expression and Regulation (CLEAR) elements in their promoters [54, 55]. The CLEAR network genes are involved in autophagosome and lysosomal biogenesis, lysosomal exocytosis, endocytosis, and membrane repair [54, 55]. Furthermore, the activation of neurological TFEB has been reported to regulate microglia-mediated degradation of A β plaques via the ALP [19, 21]. In our investigation, we found that the attenuation of AD pathology by IHT was associated with upregulated TFEB function and suppressed mTORC1 signaling. In addition, IHT upregulated TFEB nuclear translocation in PAM and improved the autophagic clearance of A β . Consistent with our findings, TFEB activation has been previously shown to increase A β clearance and lysosomal biogenesis in neurons and astrocytes in APP/PS1 mice [56]. In addition to mTORC1-related TFEB activation, SIRT1-induced TFEB deacetylation also enhances microglial phagocytosis of A β and lysosomal biogenesis [57]. Thus, increased TFEB activation in microglia leads to upregulated autophagic/lysosomal clearance of A β , thereby reducing the A β load in the brain.

An interesting thing was that the nuclear translocation of TFEB caused by TA1 was not as significant as that caused by IHT in PAM, but it still caused a significant reduction of A β plaque. Considering that TFEB is widely expressed in the central nervous system, especially in neurons, upregulation of TFEB also enhances autophagy

of APP and reduce the release of A β [58, 59]. It might contribute to the decrease of A β plaque. TA1 is used in vivo at a dose of 10 mg/kg. Song et al. proved that 10 mg/kg TA1 could be used for the treatment of AD mice [31]. He et al. also used the same dosage in studying the damage of sensory hair cells in mice [60]. Interestingly, Fig. S5 also shows that TA1 has the effect of decreasing nuclear translocation at high concentrations, suggesting that a lower concentration of TA1 may induce a higher TFEB nuclear translocation of PAM.

During late-stage AD, autophagy is typically down-regulated in PAM [13, 53, 61]. Prolonged oA β exposure has the opposite effect by impairing autophagy [62, 63]. Thus, we hypothesized that prolonged oA β stimulation causes the pro-inflammatory polarization of microglia via autophagic overload, thereby impairing microglia autophagy. After treating microglia with different durations of oA β stimulation, we observed that the microglial ability to degrade A β was significantly impaired after 12 h. Increasing research indicates that the inhibition of TFEB kinases [64–66], activation of TFEB acetylation [21], and mTOR-dependent or -independent pharmacological activation of TFEB [52, 67, 68] have therapeutic potential in AD animal models. Thus, targeting TFEB may be a promising strategy for AD treatment. In addition, many studies have demonstrated the beneficial role of IHT in treating multi-organ diseases, suggesting that IHT may serve as an adjunctive treatment for AD. However, the appropriate IHT parameters should be investigated further to achieve optimal benefits and reduce potential risks. Whether IHT has harmful or beneficial effects on other functional cells of the brain is an important reference for examining whether IHT would be available as a treatment for potential AD disorders. Therefore, the study of IHT on a variety of other cells of the nervous system deserves to be initiated.

Conclusion

The results of the present study revealed that IHT alleviates AD pathology by activating TFEB in PAM, leading to the transcriptional upregulation of the ALP that in turn improves microglia-mediated A β clearance in the brain of AD mice. This underlying mechanism highlights the potential of TFEB as a therapeutic target for AD treatment. Furthermore, compared with small-molecule TFEB activators, IHT may be a promising alternative therapeutic approach for TFEB activation that also avoids the undesired side effects of chemical drugs.

Abbreviations

A β	Beta-amyloid
AD	Alzheimer's disease
ALP	Autophagy-lysosomal pathway

A β -555	HiLyte™ Fluor 555 labeled oligomer A β 1-42
CLEAR	Coordinated Lysosomal Expression and Regulation
IHT	Intermittent hypoxia therapy
LANDO	LC3-associated endocytosis
LAMP1	Lysosomal-associated membrane protein 1
MAPK	Mitogen-activated protein kinase
mTOR	Mechanistic target of rapamycin kinase
MWM	Morris water maze
oA β	A β oligomer
PAM	Plaque-associated microglia
RPS6	Ribosomal protein S6
SEM	Standard error of measurement
TFEB	Transcription factor EB
TA1	TFEB activator 1
TG	APP/PS1 transgenic mouse
WT	Wide type

Supplementary Information

The online version contains supplementary material available at <https://doi.org/10.1186/s12974-023-02931-6>.

Additional file 1: Figure S1. Anxiety of APP/PS1 mice was not significantly improved after IHT. 8-Month-old APP/PS1 mice were treated with IHT for 28 days followed with EPM test (A to C) or OFT (D to F). (A) The trajectory of mice in EPM test for 5 min. (B) The ratio of open arm distance was calculated by the open arm distance/total distance \times 100%. (C) Time spent in open arms during EPM test. (D) The trajectory of mice in OFT for 5 min. (E) Entries to center area (small square area) in 5 min test duration. (F) Time spent in center area during OFT. $n = 6$, * $P < 0.05$, ** $P < 0.01$ and *** $P < 0.001$ by student *t* test. TG, APP/PS1 transgenic mice. **Figure S2.** IHT reduced synaptic loss in APP/PS1 mice. 8-Month-old APP/PS1 mice were treated with IHT for 28 days. (A) Brain sections of IHT mice were stained with anti-anti-synaptophysin (SYP) antibody (Abcam, ab8049) to label synaptosome. Scale bar = 100 μ m. The synaptosome content were obtained by calculating the relative area of SYP signals in cortex (B) hippocampal CA1 region (C). $n = 6$, * $P < 0.05$, ** $P < 0.01$ and *** $P < 0.001$ by two-way ANOVA. Ctx, cortex; Hipp, hippocampus. TG, APP/PS1 transgenic mice. **Figure S3.** IHT activates TFEB transcription activity. A Luciferase reporter system containing three CLEAR elements in the promoter region was constructed and transfected to HEK393T cells. Luciferase activity was determined after IHT or TA1 treatment. pGL-Basic was the empty plasmid. $n = 3$, * $P < 0.05$, ** $P < 0.01$ and *** $P < 0.001$ by student *t* test. **Figure S4.** IHT inhibits the TFEB upstream AKT–MAPK–mTOR signaling in PAM. (A and B) Proteins of mTOR, AKT, MAPK, and RPS6 and their phosphorylation levels in the hippocampus of IHT-treated APP/PS1 mice were detected by Western blot and quantified. $n = 3$ (student *t* test). (C and D) Proteins of mTOR, Akt, MAPK, and RPS6 and their phosphorylation levels of IHT-treated-in vitro PAM were detected by Western blot and quantified. $n = 3$ (two-way ANOVA). * $P < 0.05$ and *** $P < 0.001$ TG, APP/PS1 transgenic mice. **Figure S5.** Low concentration TA1 promoted nuclear translocation of TFEB. Primary microglia were treated with TA1 at indicated concentration for 12 h. TFEB was labeled by anti-TFEB antibody. Scale bar = 50 μ m. The nuclear translocation of TFEB was calculated by quantifying the TFEB intensity in DAPI positive region. At least 50 cells were counted per treatment. ** $P < 0.01$ and *** $P < 0.001$ by one-way ANOVA. **Figure S6.** IHT/TA1 activates enrichment of CLEAR element by TFEB in APP/PS1 mice brain. (A) The position indicates, where the element is located from the transcription start site. (B) Anti-TFEB antibody was used for the Chromatin Immunoprecipitation assay and quantification of immunoprecipitated DNA fragments was performed by PCR. The PCR product was obtained from the chromatin without immunoprecipitation reaction as group Input and IgG was as negative control. (C) Enrichments of the Vps35 promoter by TFEB in IHT or TA1 treated brain tissue were measured by qPCR. * $P < 0.05$ and ** $P < 0.01$ by student *t* test. **Figure S7.** TA1 enhanced TFEB nuclear translocation and upregulate the mRNA levels of TFEB target genes in vitro PAM model. Primary microglia were co-treated with 1 μ M oA β and 1 μ M TA1 for 12 h. (A, B) Cells were fixed and stained with anti-TFEB antibody and DAPI. Nuclear translocation of TFEB was measured by quantifying the intensity of TFEB in DAPI. Scale bar = 25 μ m. $n > 50$. (C–F)

mRNA levels of *Lamp1*, *Vps11*, *Wipi2*, and *Vps18* were determined by qRT-PCR. $n = 3$. * $P < 0.05$, ** $P < 0.01$ and *** $P < 0.001$ by two-way ANOVA.

Acknowledgements

We thank Professor Wenjie Luo at Cornell University for her guidance on experimental techniques. We thank Professor Chunfu Zheng at the University of Calgary (Canada) for revising and polishing this manuscript. We thank Bullet Edits Limited for the linguistic editing and proofreading of the manuscript.

Author contributions

XW and LZ contributed to the conception and design of the study. GC and YX carried out experiments, organized the database, and performed the statistical analysis. XW and YX wrote the first draft of the manuscript. YL and DW wrote sections of the manuscript. LZ completely revised the manuscript. All authors participated in reading the manuscript and approved the submitted version.

Funding

This work was supported by the National Natural Science Foundation of China [Grant number 82271914], Nantong Special Fund for Basic Research [Grant number JC12022021], and the Postgraduate Research and Practice Innovation Program of Jiangsu Province [Grant number KYCX22_3382].

Availability of data and materials

The authors confirm that the data supporting the findings of this study are available within the article and its Supplementary material. Raw data that support the findings of this study are available from the corresponding author, upon reasonable request.

Declarations

Ethics approval and consent to participate

All the study protocols of animal experiments were reviewed and approved by the Animal Care and Use Committee of Nantong University and the Jiangsu Province Animal Care Ethics Committee (approval ID: SYXK[SU]2007-0021).

Competing interests

The authors declare that they have no competing financial interests.

Author details

¹Institute of Special Environmental Medicine, Co-Innovation Center of Neuroregeneration, Nantong University, No. 9, Seyuan Road, Chongchuan District, Nantong 226009, Jiangsu, China.

Received: 4 July 2023 Accepted: 12 October 2023

Published online: 20 October 2023

References

- Li C, Gotz J. Tau-based therapies in neurodegeneration: opportunities and challenges. *Nat Rev Drug Discov*. 2017;16:863–83.
- Mullard A. Alzheimer amyloid hypothesis lives on. *Nat Rev Drug Discov*. 2016;16:3–5.
- Karran E, De Strooper B. The amyloid hypothesis in Alzheimer disease: new insights from new therapeutics. *Nat Rev Drug Discov*. 2022;21:306–18.
- Sevigny J, Chiao P, Bussiere T, Weinreb PH, Williams L, Maier M, Dunstan R, Salloway S, Chen T, Ling Y, et al. The antibody aducanumab reduces Aβeta plaques in Alzheimer's disease. *Nature*. 2016;537:50–6.
- Glymour MM, Weuve J, Dufouil C, Mayeda ER. Aduhelm, the newly approved medication for Alzheimer's disease: what epidemiologists can learn and what epidemiology can offer. *Am J Epidemiol*. 2022;191(8):1347–51.
- Gandy S, Heppner FL. Microglia as dynamic and essential components of the amyloid hypothesis. *Neuron*. 2013;78:575–7.
- Hansen DV, Hanson JE, Sheng M. Microglia in Alzheimer's disease. *J Cell Biol*. 2018;217:459–72.
- Frenkel D, Wilkinson K, Zhao L, Hickman SE, Means TK, Puckett L, Farfara D, Kingery ND, Weiner HL, El Khoury J. Scara1 deficiency impairs clearance of soluble amyloid-beta by mononuclear phagocytes and accelerates Alzheimer's-like disease progression. *Nat Commun*. 2013;4:2030.
- Zhao LN, Long H, Mu Y, Chew LY. The toxicity of amyloid beta oligomers. *Int J Mol Sci*. 2012;13:7303–27.
- Heckmann BL, Teubner BJW, Tummers B, Boada-Romero E, Harris L, Yang M, Guy CS, Zakharenko SS, Green DR. LC3-associated endocytosis facilitates beta-amyloid clearance and mitigates neurodegeneration in murine Alzheimer's disease. *Cell*. 2019;178(536–551): e514.
- Zhao Y, Wu X, Li X, Jiang LL, Gui X, Liu Y, Sun Y, Zhu B, Pina-Crespo JC, Zhang M, et al. TREM2 is a receptor for beta-amyloid that mediates microglial function. *Neuron*. 2018;97(1023–1031): e1027.
- Fyfe I. Dense-core plaques could be beneficial in AD. *Nat Rev Neurol*. 2021;17:328.
- Pomilio C, Gorjod RM, Riudavets M, Vinuesa A, Presa J, Gregosa A, Bentivegna M, Alaimo A, Alcon SP, Sevrer G, et al. Microglial autophagy is impaired by prolonged exposure to beta-amyloid peptides: evidence from experimental models and Alzheimer's disease patients. *Geroscience*. 2020;42:613–32.
- Hung C, Livesey FJ. Endolysosome and autophagy dysfunction in Alzheimer disease. *Autophagy*. 2021;17:3882–3.
- Settembre C, Di Malta C, Polito VA, Garcia Arencibia M, Vetrini F, Erdin S, Erdin SU, Huynh T, Medina D, Colella P, et al. TFEB links autophagy to lysosomal biogenesis. *Science*. 2011;332:1429–33.
- Curnock R, Calcagni A, Ballabio A, Cullen PJ. TFEB controls retromer expression in response to nutrient availability. *J Cell Biol*. 2019;218:3954–66.
- Puertollano R, Ferguson SM, Brugarolas J, Ballabio A. The complex relationship between TFEB transcription factor phosphorylation and subcellular localization. *EMBO J*. 2018;37(11):e98804.
- Ma SM, Fang ZJ, Luo WW, Yang YZ, Wang CY, Zhang Q, Wang HF, Chen HY, Chan CB, Liu ZX. The C-ETS2-TFEB axis promotes neuron survival under oxidative stress by regulating lysosome activity. *Oxid Med Cell Longev*. 2016;2016:4693703.
- Yamamoto F, Taniguchi K, Mamada N, Tamaoka A, Kametani F, Lakshmana MK, Araki W. TFEB-mediated enhancement of the autophagy-lysosomal pathway dually modulates the process of amyloid beta-protein generation in neurons. *Neuroscience*. 2019;402:11–22.
- Zheng X, Lin W, Jiang Y, Lu K, Wei W, Huo Q, Cui S, Yang X, Li M, Xu N, et al. Electroacupuncture ameliorates beta-amyloid pathology and cognitive impairment in Alzheimer disease via a novel mechanism involving activation of TFEB (transcription factor EB). *Autophagy*. 2021;17:3833–47.
- Bao J, Zheng L, Zhang Q, Li X, Zhang X, Li Z, Bai X, Zhang Z, Huo W, Zhao X, et al. Deacetylation of TFEB promotes fibrillar Aβeta degradation by upregulating lysosomal biogenesis in microglia. *Protein Cell*. 2016;7:417–33.
- Bayer U, Likar R, Pinter G, Stettner H, Demschar S, Trummer B, Neuwersch S, Glazachev O, Burtscher M. Intermittent hypoxic-hyperoxic training on cognitive performance in geriatric patients. *Alzheimers Dement (N Y)*. 2017;3:114–22.
- Chang JC, Lien CF, Lee WS, Chang HR, Hsu YC, Luo YP, Jeng JR, Hsieh JC, Yang KT. Intermittent hypoxia prevents myocardial mitochondrial Ca(2+) overload and cell death during ischemia/reperfusion: the role of reactive oxygen species. *Cells*. 2019;8:564.
- Chang JC, Hu WF, Lee WS, Lin JH, Ting PC, Chang HR, Shieh KR, Chen TI, Yang KT. Intermittent hypoxia induces autophagy to protect cardiomyocytes from endoplasmic reticulum stress and apoptosis. *Front Physiol*. 2019;10:995.
- Guo H, Ding H, Yan Y, Chen Q, Zhang J, Chen B, Cao J. Intermittent hypoxia-induced autophagy via AMPK/mTOR signaling pathway attenuates endothelial apoptosis and dysfunction in vitro. *Sleep Breath*. 2021;25:1859–65.
- Schega L, Peter B, Torpel A, Mutschler H, Isermann B, Hamacher D. Effects of intermittent hypoxia on cognitive performance and quality of life in elderly adults: a pilot study. *Gerontology*. 2013;59:316–23.
- Song S, Tan J, Miao Y, Sun Z, Zhang Q. Intermittent-hypoxia-induced autophagy activation through the ER-stress-related PERK/eIF2α/ATF4 pathway is a protective response to pancreatic β-cell apoptosis. *Cell Physiol Biochem*. 2018;51:2955–71.

28. Chi R, Chai C, Liu G, Cao H, Yang B. Chronic intermittent hypoxia-induced BNIP3 expression mitigates contractile dysfunction and myocardial injury in animal and cell model via modulating autophagy. *Hum Cell*. 2023;36:631–42.
29. Talebi M, Vadoud SAM, Haratian A, Talebi M, Farkhondeh T, Pourbagher-Shahri AM, Samarghandian S. The interplay between oxidative stress and autophagy: focus on the development of neurological diseases. *Behav Brain Funct*. 2022;18(1):3.
30. Zhao E, Czaja MJ. Transcription factor EB: a central regulator of both the autophagosome and lysosome. *Hepatology* (Baltimore, MD). 2012;55:1632–4.
31. Song JX, Malampati S, Zeng Y, Durairajan SSK, Yang CB, Tong BC, Iyaswamy A, Shang WB, Sreenivasamurthy SG, Zhu Z, et al. A small molecule transcription factor EB activator ameliorates beta-amyloid precursor protein and Tau pathology in Alzheimer's disease models. *Aging Cell*. 2020;19: e13069.
32. Ryou MG, Mallet RT, Metzger DB, Jung ME. Intermittent hypoxia training blunts cerebrocortical presenilin 1 overexpression and amyloid-beta accumulation in ethanol-withdrawn rats. *Am J Physiol Regul Integr Comp Physiol*. 2017;313:R10–8.
33. Ryou MG, Chen X, Cai M, Wang H, Jung ME, Metzger DB, Mallet RT, Shi X. Intermittent hypoxia training prevents deficient learning-memory behavior in mice modeling Alzheimer's disease: a pilot study. *Front Aging Neurosci*. 2021;13: 674688.
34. Zha L, Yu Z, Fang J, Zhou L, Guo W, Zhou J. NLR3 delays the progression of AD in APP/PS1 mice via inhibiting PI3K activation. *Oxid Med Cell Longev*. 2020;2020:5328031.
35. Kraeuter AK, Guest PC, Sarnyai Z. The open field test for measuring locomotor activity and anxiety-like behavior. *Methods Mol Biol*. 2019;1916:99–103.
36. Walf AA, Frye CA. The use of the elevated plus maze as an assay of anxiety-related behavior in rodents. *Nat Protoc*. 2007;2:322–8.
37. Wu XM, Qian C, Zhou YF, Yan YC, Luo QQ, Yung WH, Zhang FL, Jiang LR, Qian ZM, Ke Y. Bi-directionally protective communication between neurons and astrocytes under ischemia. *Redox Biol*. 2017;13:20–31.
38. Wong MY, Lewis M, Doherty JJ, Shi Y, Cashikar AG, Amelianchik A, Tymchuk S, Sullivan PM, Qian M, Covey DF, et al. 25-Hydroxycholesterol amplifies microglial IL-1beta production in an apoE isoform-dependent manner. *J Neuroinflamm*. 2020;17:192.
39. Wu X, Zhou C, Du F, Lu Y, Peng B, Chen L, Zhu L. Ginkgolide B preconditioning on astrocytes promotes neuronal survival in ischemic injury via up-regulating erythropoietin secretion. *Neurochem Int*. 2013;62:157–64.
40. Kotler SA, Ramamoorthy A. Preparation of stable amyloid-beta oligomers without perturbative methods. *Methods Mol Biol*. 2018;1777:331–8.
41. Song JX, Sun YR, Peluso I, Zeng Y, Yu X, Lu JH, Xu Z, Wang MZ, Liu LF, Huang YY, et al. A novel curcumin analog binds to and activates TFEB in vitro and in vivo independent of mTOR inhibition. *Autophagy*. 2016;12:1372–89.
42. Navarrete-Opazo A, Mitchell GS. Therapeutic potential of intermittent hypoxia: a matter of dose. *Am J Physiol Regul Integr Comp Physiol*. 2014;307:R1181–1197.
43. Shiota S, Takekawa H, Matsumoto SE, Takeda K, Nurwidya F, Yoshioka Y, Takahashi F, Hattori N, Tabira T, Mochizuki H, Takahashi K. Chronic intermittent hypoxia/reoxygenation facilitate amyloid-beta generation in mice. *J Alzheimers Dis*. 2013;37:325–33.
44. Yue X, Zhou Y, Qiao M, Zhao X, Huang X, Zhao T, Cheng X, Fan M, Zhao Y, Chen R, Zhu L. Intermittent hypoxia treatment alleviates memory impairment in the 6-month-old APP^{swe}/PS1^{dE9} mice and reduces amyloid beta accumulation and inflammation in the brain. *Alzheimers Res Ther*. 2021;13:194.
45. Meng SX, Wang B, Li WT. Intermittent hypoxia improves cognition and reduces anxiety-related behavior in APP/PS1 mice. *Brain Behav*. 2020;10: e01513.
46. McGuire M, Bradford A. Chronic intermittent hypoxia increases haematocrit and causes right ventricular hypertrophy in the rat. *Respir Physiol*. 1999;117:53–8.
47. Chiu LL, Chou SW, Cho YM, Ho HY, Ivy JL, Hunt D, Wang PS, Kuo CH. Effect of prolonged intermittent hypoxia and exercise training on glucose tolerance and muscle GLUT4 protein expression in rats. *J Biomed Sci*. 2004;11:838–46.
48. Serebrovskaya TV, Xi L. Intermittent hypoxia training as non-pharmacologic therapy for cardiovascular diseases: practical analysis on methods and equipment. *Exp Biol Med* (Maywood). 2016;241:1708–23.
49. Hanseeuw BJ, Jonas V, Jackson J, Betensky RA, Rentz DM, Johnson KA, Sperling RA, Donovan NJ. Association of anxiety with subcortical amyloidosis in cognitively normal older adults. *Mol Psychiatry*. 2020;25:2599–607.
50. Wei Z, Junhong G, Xiaoyuan N, Jie W, Zhaojun W, Meina W, Wei Y, Jun Z, Jinshun Q. Citalopram ameliorates impairments in spatial memory and synaptic plasticity in female 3xTgAD mice. *Biomed Res Int*. 2017;2017:1238687.
51. Xu Y, Jiang C, Wu J, Liu P, Deng X, Zhang Y, Peng B, Zhu Y. Ketogenic diet ameliorates cognitive impairment and neuroinflammation in a mouse model of Alzheimer's disease. *CNS Neurosci Ther*. 2022;28:580–92.
52. Cheng XH, Wei Y, Qian ZJ, Han L. Autophagy balances neuroinflammation in Alzheimer's disease. *Cell Mol Neurobiol*. 2023;43(4):1537–49.
53. Deng ZQ, Dong Y, Zhou XT, Lu JH, Yue ZY. Pharmacological modulation of autophagy for Alzheimer's disease therapy: opportunities and obstacles. *Acta Pharm Sin B*. 2022;12:1688–706.
54. Bala S, Szabo G. TFEB, a master regulator of lysosome biogenesis and autophagy, is a new player in alcoholic liver disease. *Dig Med Res*. 2018;1:16.
55. Palmieri M, Impey S, Kang H, di Ronza A, Pelz C, Sardiello M, Ballabio A. Characterization of the CLEAR network reveals an integrated control of cellular clearance pathways. *Hum Mol Genet*. 2011;20:3852–66.
56. Xiao Q, Yan P, Ma X, Liu H, Perez R, Zhu A, Gonzales E, Burchett JM, Schuler DR, Cirrito JR, et al. Enhancing astrocytic lysosome biogenesis facilitates Abeta clearance and attenuates amyloid plaque pathogenesis. *J Neurosci*. 2014;34:9607–20.
57. Zhang YD, Zhao JJ. TFEB participates in the abeta-induced pathogenesis of Alzheimer's disease by regulating the autophagy-lysosome pathway. *DNA Cell Biol*. 2015;34:661–8.
58. Xiao Q, Yan P, Ma X, Liu H, Perez R, Zhu A, Gonzales E, Tripoli DL, Czerniewski L, Ballabio A, et al. Neuronal-targeted TFEB accelerates lysosomal degradation of APP, reducing Aβ generation and amyloid plaque pathogenesis. *J Neurosci*. 2015;35:12137–51.
59. Yamamoto F, Taniguchi K, Mamada N, Tamaoka A, Kametani F, Lakshmana MK, Araki W. TFEB-mediated enhancement of the autophagy-lysosomal pathway dually modulates the process of amyloid β-protein generation in neurons. *Neuroscience*. 2019;402:11–22.
60. He W, Wu F, Xiong H, Zeng J, Gao Y, Cai Z, Pang J, Zheng Y. Promoting TFEB nuclear localization with curcumin analog C1 attenuates sensory hair cell injury and delays age-related hearing loss in C57BL/6 mice. *Neurotoxicology*. 2023;95:218–31.
61. Pomilio C, Pavia P, Gorjod RM, Vinuesa A, Alaimo A, Galvan V, Kotler ML, Beauquis J, Saravia F. Glial alterations from early to late stages in a model of Alzheimer's disease: evidence of autophagy involvement in a beta internalization. *Hippocampus*. 2016;26:194–210.
62. Pan XD, Zhu YG, Lin N, Zhang J, Ye QY, Huang HP, Chen XC. Microglial phagocytosis induced by fibrillar beta-amyloid is attenuated by oligomeric beta-amyloid: implications for Alzheimer's disease. *Mol Neurodegener*. 2011;6:45.
63. Chilakala RR, Manchikalapudi AL, Kumar A, Sunkaria A. Sulforaphane attenuates a beta oligomers mediated decrease in phagocytic activity of microglial cells. *Neuroscience*. 2020;429:225–34.
64. Zhou J, Tan SH, Nicolas V, Bauvy C, Yang ND, Zhang JB, Xue Y, Codogno P, Shen HM. Activation of lysosomal function in the course of autophagy via mTORC1 suppression and autophagosome-lysosome fusion. *Cell Res*. 2013;23:508–23.
65. Chun YS, Kim MY, Lee SY, Kim MJ, Hong TJ, Jeon JK, Ganbat D, Kim HT, Kim SS, Kam TI, Han S. MEK1/2 inhibition rescues neurodegeneration by TFEB-mediated activation of autophagic lysosomal function in a model of Alzheimer's Disease. *Mol Psychiatry*. 2022;27(11):4770–80.
66. Tan A, Prasad R, Lee C, Jho EH. Past, present, and future perspectives of transcription factor EB (TFEB): mechanisms of regulation and association with disease. *Cell Death Differ*. 2022;29:1433–49.
67. Sun YX, Ji XM, Mao XO, Xie L, Jia JP, Galvan V, Greenberg DA, Jin KL. Differential activation of mTOR complex 1 signaling in human brain with mild to severe Alzheimer's disease. *J Alzheimers Dis*. 2014;38:437–44.

68. Song HC, Chen Y, Chen YQ, Park J, Zheng M, Surh YJ, Kim UH, Park JW, Yu R, Chung HT, Joe Y. GSK-3 beta inhibition by curcumin mitigates amyloidogenesis via TFEB activation and anti-oxidative activity in human neuroblastoma cells. *Free Radic Res.* 2020;54:918–30.

Publisher's Note

Springer Nature remains neutral with regard to jurisdictional claims in published maps and institutional affiliations.

Ready to submit your research? Choose BMC and benefit from:

- fast, convenient online submission
- thorough peer review by experienced researchers in your field
- rapid publication on acceptance
- support for research data, including large and complex data types
- gold Open Access which fosters wider collaboration and increased citations
- maximum visibility for your research: over 100M website views per year

At BMC, research is always in progress.

Learn more biomedcentral.com/submissions

